

NOMA-Enabled Dual-IRS Relay Network Integrated with Ambient Backscatter Communication

1st Chandrima Thakur

Kolkata, India

chandrima31.ece@gmail.com

2nd Priyanka Ghosh

Dept. of ECE
NIT, Durgapur
India

priyankaghoshdey01@gmail.com

3rd Rashmita Badhai

Dept. of ECE
NIT, Durgapur
India

rb.24ec1109@nitdgp.ac.in

4th Sumit Kundu

Dept. of ECE
NIT, Durgapur
India

skundu.ece@nitdgp.ac.in

Abstract

This paper analyzes a NOMA-enabled dual-Intelligent Reflecting Surface (IRS) relay network integrated with Ambient Backscatter (BS) communication. The system comprises a source, an energy-constrained relay with energy harvesting (EH) and BS capabilities, two NOMA users, and a BS node. The relay adopts a time-switching relaying (TSR) protocol to harvest energy and forward information, while simultaneously enabling BS-based communication. Two IRS are deployed to enhance the S—R and R—→(DI, D2) links under blockage conditions. Closed-form expressions for the Outage Probability (OP) and Throughput of both the main communication links and the BS-assisted secondary links are derived. Furthermore, throughput is analyzed under varying system parameters, including power allocation factors, reflection efficiency, IRS elements, and transmission rate. Monte Carlo simulations validate the analytical results. Numerical findings reveal critical trade-offs between the main and RS links. The proposed framework provides useful insights for designing reliable and energy-efficient NOMA-IRS-aided BS networks for future IoT applications.

Index Terms

NOMA, PSR, Energy harvesting, IRS, Backscatter,

I. INTRODUCTION

The rapid proliferation of Internet of Things (IoT) devices and the growing demand for high data rates have accelerated the evolution of next-generation wireless communication systems. To meet the ever-increasing connectivity and energy efficiency requirements, several promising technologies such as Non-Orthogonal Multiple Access (NOMA), Intelligent Reflecting Surfaces (IRSs), and Ambient Backscatter Communication (AmBC) have emerged as key enablers for beyond-5G and 6G networks.

NOMA, a vital 5G technology, allows multiple users to share time-frequency resources. However, its performance degrades in challenging environments, especially for far users. Cooperative NOMA (CR-NOMA) addresses this by using relays to assist weak users, but half-duplex relaying with near users reduces spectral efficiency due to time slot division [2]. Ambient backscatter (AmBack) communication is a promising way to enable low-power, green IoT connectivity by allowing devices to transmit data by reflecting ambient RF signals. [3] It reduces power consumption, eliminates the need for dedicated transmitters, avoids energy-intensive hardware, and requires no additional spectrum allocation. Hence, integrating AmBack communication into NOMA-enabled networks can significantly enhance system capacity and spectral efficiency [4]. A backscatter-enabled NOMA network is proposed in [5], where BDs transmit by modulating existing signals. Additionally, [6] explore hybrid relaying strategies and outage performance under practical constraints like nonlinear energy harvesting and hardware impairments.

IRS have recently gained attention for enhancing wireless network performance by intelligently reflecting electromagnetic waves. Acting as passive beamformers, IRS can extend coverage, focus energy toward users, and reduce interference. When integrated into AmBack-enabled NOMA networks, RIS improves communication with cell-edge users, reduces energy consumption due to its passive nature, and enhances spectral efficiency without self-interference. A theoretical framework for evaluating outage probability, symbol error rate, and ergodic capacity is proposed in [7], comparing IRS-assisted and AF relaying systems. Results show that IRS-assisted systems outperform AF-based ones. Study in [8], [9] shows RIS integration significantly improves traditional AmBack system performance and increasing RIS elements further improves outage probability. In [10], an alternating optimization method with a difference-of-convex algorithm shows that RIS-assisted full-duplex backscatter communication offers notable power savings over half-duplex setups.

In [11], a two-time-slot transmission model is analyzed, where the near user receives the NOMA signal in the first slot, and the far user is served in the second. This prevents the far user from utilizing the entire frame, limiting its performance. Introducing a RIS between the source and the far user can allow signal reflection during the first slot, improving reception and spectral efficiency. In [12], a RIS-assisted IR network is evaluated using conventional and accumulated energy harvesting under a TSR protocol. However, it does not explore support for low-power secondary IoT links. Reconfiguring the near user

as a hybrid backscatter node could address this gap. In [15], this work investigates the performance of multiple IRS-assisted wireless networks over Nakagami-m fading channels, deriving analytical outage probability expressions and demonstrating how system reliability improves with optimized IRS deployment. In [16], this work studies a NOMA network assisted by two reconfigurable intelligent surfaces and provides analytical performance analysis. The results demonstrate how employing dual RIS can significantly improve signal strength, enhance spectral efficiency, and reduce outage probability in NOMA-based wireless communication systems.

In [17], this work investigates communication systems employing two reconfigurable intelligent surfaces (RIS) combined with a decode-and-forward (DF) relay to enhance coverage. The study analyzes system performance and reveals conditions under which using a single relay remains sufficient, uncovering key trade-offs between RIS deployment, relay assistance, and achievable network coverage. In [18], this work examines a wireless-powered communication system enhanced by two reconfigurable intelligent surfaces to improve physical layer security. Analytical secrecy performance expressions are derived, showing that double-RIS deployment can greatly enhance secure transmission in Rayleigh fading environments. In [19], this work studies cooperative NOMA systems assisted by an intelligent reflecting surface and employs particle swarm optimization to jointly optimize system parameters. The results show that IRS integration and intelligent parameter tuning significantly enhance system throughput and energy efficiency.

Motivated by the above observations, this paper investigates a NOMA-enabled dual-IRS relay network integrated with AmBC. In this system, the source communicates with two NOMA users via an energy-constrained relay equipped with both EH and backscatter capabilities. Two IRSs are deployed to enhance the S–R and R–(D_1, D_2) links, particularly under blockage conditions. The main contributions of this paper are summarized as follows:

- We propose a novel dual-IRS-assisted NOMA relay network architecture integrated with AmBC and energy harvesting. The relay employs a TSR protocol to simultaneously harvest energy and support backscatter-based communication.
- Closed-form expressions for the outage probability (OP) and throughput of both the main and backscatter-assisted links are derived.
- MATLAB simulations validate the analytical derivations and reveal crucial trade-offs between the main and backscatter links, providing valuable insights for designing outage probability and throughput for NOMA–IRS–AmBC networks.

This paper is organized as follows: Section II the system model and derives the relevant signal-to-interference-plus-noise ratio (SINR) expressions. In Section III, we present the analytical formulations for the individual outage probabilities and throughput of the main link and the BS link. Section IV provides both analytical and MATLAB-based simulation results to validate the proposed framework. Finally, Section V concludes the paper with key findings and potential future directions.

II. SYSTEM MODEL

Fig. 1 illustrates a NOMA-enabled dual-IRS relay network comprising a source S, relay R, two NOMA-enabled users D_1 and D_2 , and two IRS arrays I_1 and I_2 . The source S is equipped with a constant power supply, whereas relay R is energy constrained with EH and BS capabilities. In addition to relaying $S \rightarrow D_1$ and $S \rightarrow D_2$ communication, node R communicates with node C using BS technology. IRS I_1 and I_2 are deployed at specific locations to assist the communications from S to R and from R to $\{D_1, D_2\}$ respectively. Direct $S \rightarrow \{D_1, D_2\}$ communication is not available due to possible blockage or severe path-loss. Moreover, due to blockage between I_1 and I_2 , there is no effective communication link between them. Reflections from I_1 and I_2 are considered only once, while higher-order reflections are omitted. In the sequel, the subscripts S, R, D_1, D_2, I_1 and I_2 denote the source, relay, near user, far user, IRS1, and IRS2, respectively. Each node is equipped with a single omnidirectional antenna operating in half-duplex mode. IRSs I_1 and I_2 are equipped with N and M reflecting elements, respectively. As shown in Fig.2, the whole communication procedure is divided into two phases. In Phase I, the source S transmits its information to the relay R via IRS I_1 during time slot t_1 . Concurrently, relay R harvests energy and decodes the received signal while simultaneously backscattering it to transmit its own information to node C. Relay R employs the Power Splitting Relaying (PSR) technique, where a fraction ρ of the received power is allocated to the BS interface for backscattering, and the remaining fraction $(1-\rho)$ is dedicated to the EH/Information Decoding (ID) interface. Relay R performs these operations using two separate interfaces, i.e., a BS interface and an EH/ID interface. In Phase II, using the harvested energy, relay R forwards the decoded source signal to D_1 and D_2 via IRS I_2 . Meanwhile, C acts as a BS transmitter and communicates with R by backscattering the received ambient signal. It can be observed that, in both phases, the relay node operates in full-duplex mode, simultaneously supporting the primary $S \rightarrow \{D_1, D_2\}$ communication and the secondary BS-based $R \leftrightarrow C$ link.

A. Mathematical Modeling

1) *Phase I*: In Phase I, S transmits a superimposed signal in the first half of a time block given as:

$$s = \sqrt{a_1}x_1 + \sqrt{a_2}x_2 \quad (1)$$

$$a_1 + a_2 = 1,$$

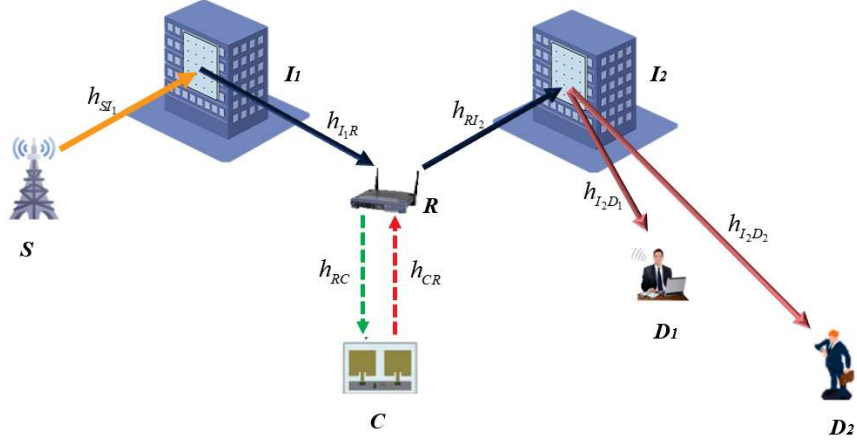


Fig. 1. System Model for NOMA-Enabled Dual-IRS Relay Network with Backscatter Communication

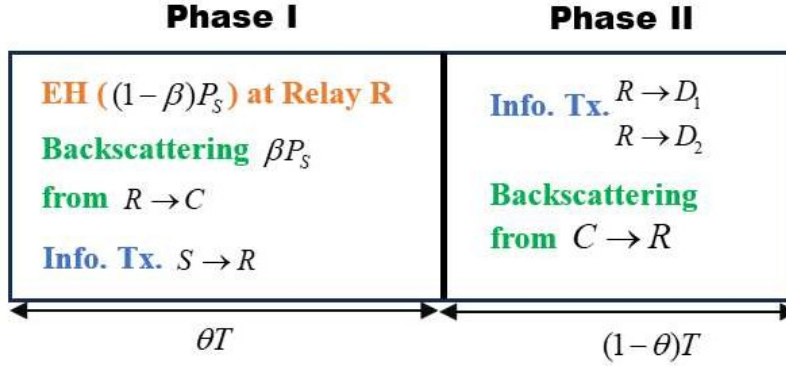


Fig. 2. Time frame structure of the proposed transmission protocol

$$a_1, a_2 \geq 0,$$

where a_1 and a_2 are the power allocation coefficients at R for x_1 and x_2 , respectively.

Initially, the RIS reflects the incident signal to R. The received signal at R is represented as:

$$y_R = \sqrt{P_S} (h_{S I_1}^T \Theta h_{I_1 R}) s + n = \sqrt{P_S} h_1 s + n \quad (2)$$

where P_S is the transmit power at S,

$$\Theta_1 = \text{diag}(\eta_{11} e^{j\theta_{1,1}}, \dots, \eta_{1N} e^{j\theta_{1,N}})$$

denotes the reflection coefficient matrix of RIS_1 with $\theta_1 \in [0, 1]$ denoting the phase shift and the reflection coefficient of the i -th reflecting element of RIS_1 , respectively. $h_{S I_1} \in \mathbb{C}^{N \times 1}$ is the channel vector from S to RIS_1 ; $h_{I_1 R} \in \mathbb{C}^{N \times 1}$ is the channel vector from RIS_1 to R; n denotes AWGN at R.

The effective channel coefficient of the first-hop can be rewritten as:

$$h_1 \triangleq \mathbf{h}_{1R}^T \Theta_1 \mathbf{h}_{S1} = \sum_{i=1}^N \eta_{1i} |h_{S1,i}| |h_{R,i}| e^{j(\theta_{S1,i} + \theta_{1,i} + \theta_{R,i})} \quad (3)$$

where h_{S_i} is the channel coefficient from S to the i -th reflecting element of RIS_1 , h_{iR} is the channel coefficient from the i -th reflecting element of RIS_1 to R, and $\theta_{S_i}, \theta_{iR}$ are their respective phases. For the PS-based protocol, $(1-\beta)$ part of the received signal at R will be assigned for EH:

$$y_R^{\text{EH}} = \sqrt{1-\beta} y_R \quad (4)$$

Thus, the energy harvested by R during the first-hop is:

$$E_R = \eta(1-\beta)P_s |h_1|^2 \theta T, \quad (5)$$

where η denotes the energy conversion efficiency and θ is the EH time fraction. The power transmitted by R is given as:

$$P_R = \frac{E_R}{(1-\theta)T} = \frac{(1-\beta)\eta P_S |h_1|^2 \theta}{(1-\theta)} \quad (6)$$

SNR at R to decode x_1 and x_2 :

$$\gamma_{SR}^{(x_1)} = \frac{\alpha_1 P_S |h_1|^2}{\alpha_2 P_S |h_1|^2 + N_0} \quad (7)$$

$$\gamma_{SR}^{(x_2)} = \frac{\alpha_2 P_S |h_1|^2}{N_0} \quad (8)$$

Meanwhile, R also transfers its information to C (BS receiver) by backscattering:

$$P_R^{BS} = \beta \zeta P_S |h_1|^2 \quad (9)$$

where ζ is the backscattering efficiency. The received SNR at C is:

$$\gamma_{RC}^{BS} = \frac{\beta \zeta P_S |h_1|^2 |h_{RC}|^2}{N_0} \quad (10)$$

2) *Phase II*: During the second phase, i.e., duration $(1-\theta)T$, the relay R uses the energy harvested in Phase I to forward the decoded signal to the destination users D_1 and D_2 via I_2 expressed as:

$$s = \sqrt{b_1} x_1 + \sqrt{b_2} x_2 \quad (11)$$

$$b_1 + b_2 = 1,$$

$$b_1, b_2 \geq 0,$$

where b_1 and b_2 are the power allocation coefficients at R. The signal received at D_k is:

$$y_{D_k} = \sqrt{P_R} (h_{RI_2}^T \Theta_2 h_{I_2 D_k}) s_R + n = \sqrt{P_R} h_{2k} s_R + n \quad (12)$$

where

$$\Theta_2 = \text{diag}(\eta_{21} e^{j\theta_{2,1}}, \dots, \eta_{2M} e^{j\theta_{2,M}})$$

denotes the reflection coefficient matrix of IRS I_2 with $\theta_{2i} \in [0, 2\pi]$ denoting the phase shift and η_{2i} the reflection coefficient of the i -th reflecting element of I_2 , respectively. Moreover, $h_{RI_2} \in \mathbb{C}^{M \times 1}$ is the channel vector from R to I_2 , and $h_{I_2 D_k} \in \mathbb{C}^{M \times 1}$ is the channel vector from I_2 to D_k .

The effective channel coefficient of the second hop is given by:

$$h_{RI_2}^T \Theta_2 h_{I_2 D_k} \quad (13)$$

which can be rewritten as

$$h_{2k} \triangleq h_{RI_2}^T \Theta_2 h_{I_2 D_k} = \sum_{i=1}^M \eta_{2i} |h_{Ri}| |h_{iD_k}| e^{j(\theta_{Ri} + \theta_{2i} + \theta_{iD_k})} \quad (14)$$

where h_{Ri} is the channel coefficient from R to the i -th reflecting element of I_2 , h_{iD_k} is the channel coefficient from the i -th reflecting element of IRS I_2 to destination D_k , $\theta_{Ri}, \theta_{iD_k}$ are the phases of h_{Ri} and h_{iD_k} , respectively, and η_{2i} is the reflection amplitude of the i -th reflecting element.

Decoding at D_1 and D_2 : Since D_1 is the near user, it first decodes x_2 treating x_1 as interference:

$$\gamma_{RD_1}^{(x_2)} = \frac{\alpha_2 P_R g_{RD_1}}{\alpha_2 P_R g_{RD_1} + N_0} \quad (15)$$

Then, D_1 decodes x_1 :

$$\gamma_{RD_1}^{(x_1)} = \frac{\alpha_1 P_R g_{RD_1}}{N_0} \quad (16)$$

D_2 being the far user, directly decodes x_2 treating x_1 as interference:

$$\gamma_{RD_2}^{(x_2)} = \frac{\alpha_2 P_R g_{RD_2}}{N_0 + I_{CD_2}} \quad (17)$$

where,

$$I_{CD_2} = \zeta \sqrt{P_R g_{RC} g_{CD_2}} \quad (18)$$

is the interference from C to D_2 .

The overall SNR of the main link involves two hops: from S to R and from R to both D_1 and D_2 . Therefore, the overall SNR of the links $S \rightarrow D_1$ and $S \rightarrow D_2$ is expressed as

$$\gamma_{D_1} = \min(\gamma_{SR}^{(x_1)}, \gamma_{RD_1}^{(x_1)}) \quad (19)$$

$$\gamma_{D_2} = \min(\gamma_{SR}^{(x_2)}, \gamma_{RD_2}^{(x_2)}) \quad (20)$$

where γ_{SR} denotes the SNR of the $S \rightarrow R$ hop, γ_{RD} , the SNR of the $R \rightarrow D_1$ hop and γ_{RD_2} , the SNR of the $R \rightarrow D_2$ hop.

Similarly, as a result of backscattering operation at C (i.e., secondary communication during Phase II), the received SNR at node R can be written as:

$$\gamma_{CR}^{BS} = \frac{\eta \zeta P_S g_{SR} g_{RC} g_{CR}}{N_0} \quad (21)$$

III. PERFORMANCE ANALYSIS

In this section, we derive the closed-form expressions for the outage probability (OP) and throughput of the proposed scheme. The overall network OP for the main link is expressed as

$$P_{out}^{Main} = P_{out}^{(D_1)} + P_{out}^{(D_2)} \quad (22)$$

where, $P_{out}^{(D_1)}$ and $P_{out}^{(D_2)}$ represent the OP for D_1 and D_2 , respectively.

A. Outage Probability Analysis of Main Link (S to D_1 and D_2)

The outage probability for D_1 is given by

$$\begin{aligned} P_{out}^{D_1} &= Pr(\gamma_{D_1} < \gamma_{th}^D) \\ &= Pr(\min(\gamma_{SR}^{(x_1)}, \gamma_{RD_1}^{(x_1)}) < \gamma_{th}^D) \\ &= 1 - \underbrace{P(\gamma_{SR}^{(x_1)} \geq \gamma_{th}^D)}_{A_1} \cdot \underbrace{P(\gamma_{RD_1}^{(x_1)} \geq \gamma_{th}^D)}_{A_2}. \end{aligned} \quad (23)$$

Proposition 1: According to (23), the OP of $S \rightarrow D_1$ can be expressed as

$$P_{out}^{D_1} = 1 - (1 - A_1)(1 - A_2), \quad (24)$$

where,

$$A_1 = \frac{\gamma(N, \tau_1)}{\Gamma(N)}, A_2 = \Phi\left(\frac{\log(\tau_2) - 2\mu_x}{\sqrt{2}\sigma_x}\right) \quad (25)$$

Here,

$$\tau_1 = \frac{\gamma_{th}^D N_0 \lambda_{SR}}{(\alpha_1 - \alpha_2 \gamma_{th}^D) P_S}, \quad (26)$$

$$\tau_2 = \frac{(1 - \theta) \gamma_{th}^D}{\alpha_1 P_S (1 - \beta) \theta_\eta}, \quad (27)$$

and $\Gamma(\cdot)$ is the standard normal CDF. Similarly, the OP of $S \rightarrow D_2$ link is expressed as

$$P_{out}^{D_2} = 1 - (1 - B_1)(1 - B_2), \quad (28)$$

where,

$$B_1 = \frac{\gamma(N, \tau_3)}{\Gamma(N)}, B_2 = \Phi\left(\frac{\log(\tau_4) - 2\mu_y}{\sqrt{2}\sigma_y}\right) \quad (29)$$

Here,

$$\tau_3 = \frac{\gamma_{th}^D N_0 \lambda_{SR}}{\alpha_2 P_S}, \quad (30)$$

$$\tau_4 = \frac{(1 - \theta) \gamma_{th}^D}{\alpha_2 P_S (1 - \beta) \theta_\eta}, \quad (31)$$

The detailed derivation has been presented in Appendix A.

B. Outage Probability Analysis of BS Link (R-C and C-R)

The OP expression for the R-C link is given as

$$P_{\text{out}}^{RC} = Pr(\gamma_{RC} < \gamma_C^{\text{th}}) \approx \Phi\left(\frac{\log(\tau_5) - 2\mu_z}{\sqrt{2}\sigma_z}\right). \quad (32)$$

Where,

$$\tau_5 = \frac{\gamma_{\text{th}}^C N_0}{\zeta(1-\beta)P_S}, \mu_z = \log\left(\frac{N^2}{\sqrt{N^2 + 2N}}\right), \sigma_z^2 = \log\left(1 + \frac{2}{N}\right). \quad (33)$$

Similarly, the OP expression for the C-R link is given as,

$$P_{\text{out}}^{CR} = Pr(\gamma_{CR} < \gamma_C^{\text{th}}) \approx \Phi\left(\frac{\log(\tau_6) - 2\mu_w}{\sqrt{2}\sigma_w}\right), \quad (34)$$

Where,

$$\tau_6 = \frac{\gamma_{\text{th}}^C N_0}{\zeta(1-\theta)(1-\beta)P_S}, \mu_w = \log\left(\frac{N^2}{\sqrt{4N^2 + 4N}}\right), \sigma_w^2 = \log\left(4 + \frac{4}{N}\right). \quad (35)$$

The detailed derivation has been presented in Appendix B.

C. Throughput of the Main link)

The total throughput of the main NOMA link is the sum of throughputs for both users:

$$\begin{aligned} C_T^{\text{Main}} &= C_T^{D_1} + C_T^{D_2} \\ \Rightarrow C_T^{\text{Main}} &= (1 - P_{\text{out}}^{D_1})U + (1 - P_{\text{out}}^{D_2})U \end{aligned}$$

D. Throughput of the BS link

The total throughput of the backscatter system is

$$\begin{aligned} C_T^{\text{BS}} &= C_T^{RC} + C_T^{CR} \\ \Rightarrow C_T^{\text{BS}} &= (1 - P_{\text{out}}^{RC})\bar{U} + (1 - P_{\text{out}}^{CR})\bar{U} \end{aligned}$$

IV. RESULTS AND ANALYSIS

In this research, we used MATLAB Version 9.1.0.813654 (R2023b) to simulate the plots. Monte Carlo simulation is used to investigate the developed analysis. The parameters used in simulation are listed in Table 1.

TABLE I
SIMULATION PARAMETERS

Parameter	Description	Value
N, M	Number of IRS elements	4, 4
η_α	Energy Harvesting Efficiency	0.7
θ	Time Splitting Coefficient	0.5
β	BS Reflection Coefficient	0.7
ζ	BS Reflection Efficiency	0.3
U, \bar{U}	Transmission Rates	2, 0.5 bit/s/Hz

Fig. 3 illustrates the throughput performance as a function of the transmission rate for the conventional legacy scheme and the proposed Dual-IRS aided BS scheme, that incorporates both main and BS communication links. From Fig. 3 it is observed that the analytical results match the simulation results thereby verifying the accuracy of our analysis. Moreover, the legacy scheme outperforms both the main and backscatter links in terms of throughput, as it is free from BS interference. It is also found that the throughput for each link initially increases with the transmission rate due to higher spectral efficiency, but after a certain point, it starts declining due to increased OP. In the proposed scheme, the degradation in throughput is primarily caused by interference from the BS transmission during the second time slot, which reduces the effective SINR at the destination.

Fig. 4 presents the throughput performance of three communication schemes: Legacy, Main Link (via Dual IRS-aided relay), and Backscatter Link as a function of the time-splitting factor θ . Initially, as θ increases from 0, the throughput improves for all links due to improved EH, which in turn strengthens the transmitted and backscattered signals. However, beyond a certain optimal point, further increase in θ begins to decrease the effective transmission duration, leading to a decrease in throughput. As θ increases, the threshold SNR required for successful decoding decreases, due to increased energy available at the nodes. Consequently, the outage probability reduces, and the throughput improves. However, for large values of θ , insufficient time for information transmission becomes the dominant limiting factor, thereby reducing throughput. In the figure, the legacy system

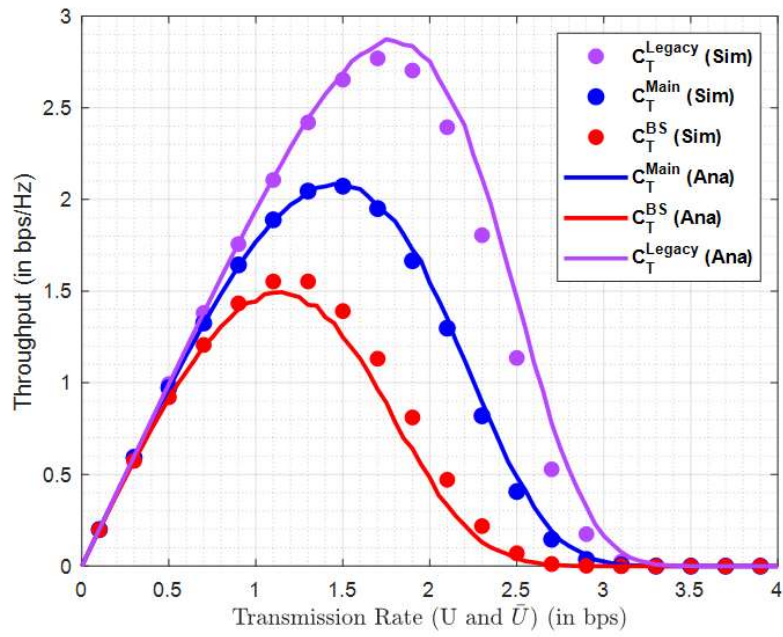


Fig. 3. Throughput versus Transmission Rate for Legacy, Main and Backscatter(BS) Links

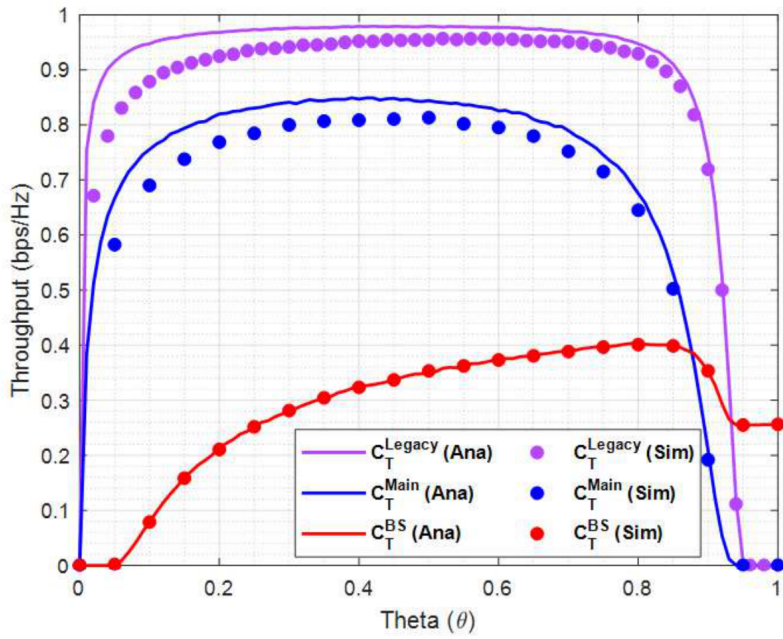


Fig. 4. Throughput versus θ for Legacy scheme, Main and Backscatter Links

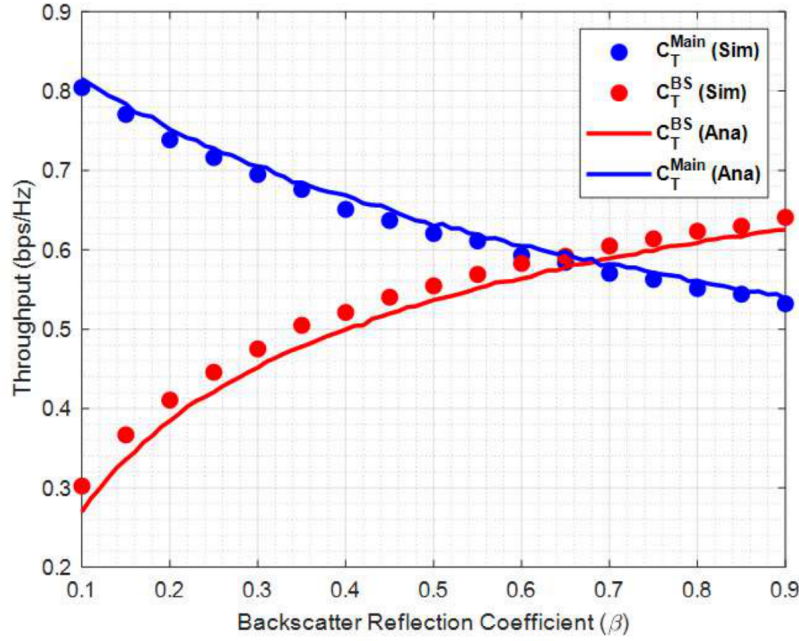


Fig. 5. Throughput versus β for Main and BS Links

achieves the highest throughput across all values of β , without any secondary link interference. Compared to the main link, the backscatter link has lower throughput.

Fig. 5 illustrates the impact of the backscatter reflection coefficient β on the throughput performance of main and BS links. It is shown that as the value of β increases, throughput of BS link increases while the main link experiences increasing interference and a consequent drop in throughput. At higher values of β , a larger portion of the received signal power is reflected back by R which leads to improved SNR and improved throughput at C. At around $\beta=0.55$, both main and BS links achieve comparable throughput. Beyond this point, BS link becomes stronger than the main link. This highlights a critical trade-off in the proposed Dual IRS-aided BS system, where increasing the BS performance can impair the main communication reliability.

Fig. 6 presents the variation of OP with respect to SNR for both the main link and the BS link, under different IRS configurations. Specifically, the figure compares several scenarios by varying the number of reflecting elements in t (N) and r (M). The curves demonstrate the effect of IRS diversity on the link reliability. It is found that the main links consistently outperform the BS links across all SNR values. Increasing N leads to a significant improvement in throughput in the main link while the BS link relies on the relay's harvested energy and are unaffected by changes in M . Among the configurations, the main link with $N=8$, $M=8$ delivers the best performance, achieving the lowest outage probability while the BS link with $N=4$, $M=4$ shows the highest OP across the entire SNR range.

Fig. 7 illustrates the impact of the number of IRS elements on the outage performance of both the main and BS communication links, under different values of BS reflection efficiency β . The plots present both analytical and simulation results, which exhibit a close match across all configurations, thereby validating the accuracy of the theoretical analysis. It is observed that as the number of IRS elements increases, the outage probability consistently decreases for both main and BS links. However, while increasing N benefits the BS link, it simultaneously introduces interference to the main link, which can offset some of the gains in reliability. For the BS link, as β increases from 0.3 to 0.5, it significantly improves the network performance. This is because a higher reflection efficiency implies that the backscatter device reflects a greater portion of the incident signal energy which results in a stronger backscattered signal, reducing the OP by improving the SNR at the backscatter receiver. Conversely, for the main link, increasing β from 0.3 to 0.5 leads to a slightly higher OP. This is because, as the backscattered signal becomes more powerful, it causes more disruption to the primary signal reception, especially when node C reflects with higher efficiency.

V. CONCLUSION

A two users NOMA based transmission enabled by dual RIS and a hybrid energy harvesting relay based on PSR is analyzed. There is a backscattered based communication between the relay(R) and BS node(C) is investigated with the RIS based network. The Throughput of dual RIS with BS integrated network is lower than that of dual RIS in absence of BS, as backscattering

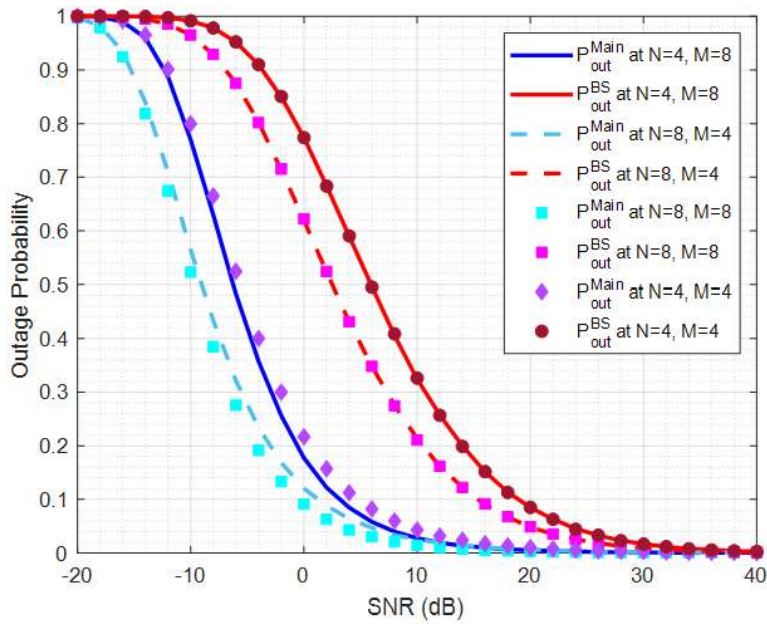


Fig. 6. Outage Probability versus SNR for Main and Backscatter (BS) communication links under varying number of IRS elements: IRS1 with N elements and IRS2 with M elements

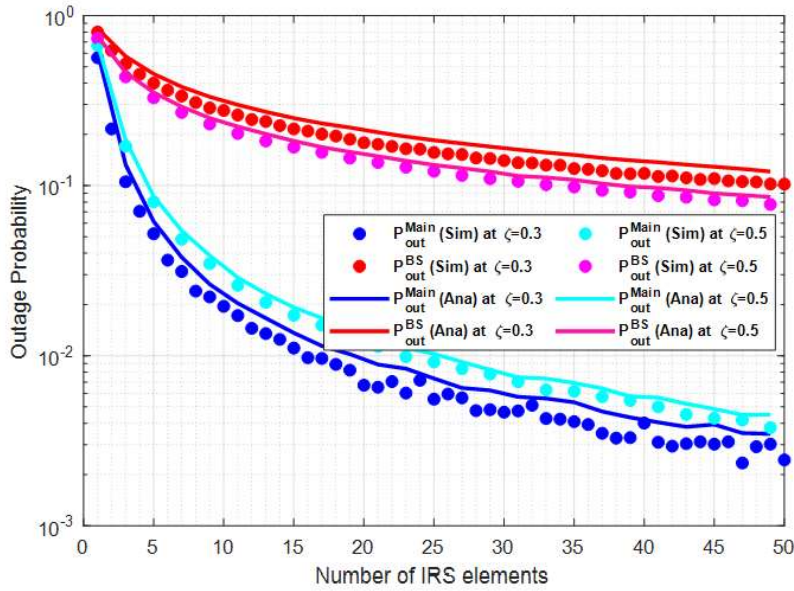


Fig. 7. Outage Probability versus number of IRS elements for both Main and BS links w.r.t different values of BS reflection efficiency, ζ

from C causes interference at D_1 and D_2 . Increase in backscatter coefficient (β) increases throughput of BS link, but reduces throughput of main two users network due to interference from C. Outage probability of main network as well as BS network reduces with increase in RIS elements. Higher RIS elements in first RIS increases the transmit power of relay and enhances throughput of BS link. The study is useful in designing *multi-RIS* network with energy harvesting relay integrated with backscattering network for IOT applications.

REFERENCES

- [1] B. Qian, H. Zhou, T. Ma, K. Yu, Q. Yu, and X. Shen, "Multi-operator spectrum sharing for massive IoT coexisting in 5G/B5G wireless networks," *IEEE J. Sel. Areas Commun.*, vol. 39, no. 3, pp. 881–895, Mar. 2021.
- [2] M. Zeng, W. Hao, O. A. Dobre, and Z. Ding, "Cooperative NOMA: State of the Art, Key Techniques, and Open Challenges," *IEEE Network*, vol. 34, no. 5, pp. 205–211, Sep./Oct. 2020, doi: 10.1109/MNET.011.1900601.
- [3] P. Ghosh, H. Yenna, S. D. Roy and S. Kundu, "Outage Analysis of an EH Relay aided Network with Ambient-Backscattering," 2024 IEEE International Conference on Electronics, Computing and Communication Technologies (CONECCT), Bangalore, India, 2024, pp. 1–6, doi: 10.1109/CONECCT62155.2024.10677243.
- [4] W. Chen, H. Ding, S. Wang, D. B. da Costa, F. Gong, and P. H. J. Nardelli, "Backscatter cooperation in NOMA communications systems," *IEEE Trans. Wireless Commun.*, vol. 20, no. 6, pp. 3458–3474, Jun. 2021.
- [5] Q. Zhang, L. Zhang, Y.-C. Liang, and P.-Y. Kam, "Backscatter-NOMA: A Symbiotic System of Cellular and Internet-of-Things Networks," *IEEE Access*, vol. 7, pp. 20000–20013, 2019, doi: 10.1109/ACCESS.2019.2897822.
- [6] S. Bisen, J. Jose, V. Bhatia, A. K. Mishra, and K. Choi, "Hybrid backscatter NOMA under imperfect CSI and hardware impairment," *IEEE Commun. Lett.*, vol. 27, no. 11, pp. 3078–3082, 2023.
- [7] A.-A. A. Boulogeorgos and A. Alexiou, "Performance analysis of reconfigurable intelligent surface-assisted wireless systems and comparison with relaying," *IEEE Access*, vol. 8, pp. 94463–94483, 2020.
- [8] U. S. Toro, M. Elsayed, B. M. ElHalawany, and K. Wu, "Performance analysis of intelligent reflecting surfaces in ambient backscattering NOMA systems," *IEEE Trans. Veh. Technol.*, 2023.
- [9] A. T. Le, T. N. Nguyen, L. T. Tu, T. P. Tran, T. T. Duy, M. Voznak, and Z. Ding, "Performance analysis of RIS-assisted ambient backscatter communication systems," *IEEE Wireless Commun. Lett.*, 2023.
- [10] Z. Tu, R. Long, Y. Pei, and Y.-C. Liang, "RIS-enabled full-duplex backscatter communication in multi-user symbiotic radio," *IEEE Trans. Wireless Commun.*, 2024.
- [11] S. Bisen and V. Bhatia, "Performance analysis of backscatter-based coordinated direct and relay transmission with NOMA," in *Proc. IEEE Wireless Commun. Netw. Conf. (WCNC)*, Mar. 2023, pp. 1–6.
- [12] P. Ghosh, S. D. Roy, and S. Kundu, "Outage Analysis of an Incremental Relaying aided Accumulated Energy harvesting based Two Users NOMA Network assisted by an IRS," in *Proc. IEEE Nat. Conf. Commun. (NCC)*, 2025.
- [13] Janghel, Komal, "Performance analysis of IRS assisted underlay cognitive radio networks," in *IEEE 19th India Council International Conference (INDICON)*, pp. [1–5], [2022].
- [14] A. A. Nasir, X. Zhou, S. Durrani and R. A. Kennedy, "Relaying Protocols for Wireless Energy Harvesting and Information Processing," in *IEEE Transactions on Wireless Communications*, vol. 12, no. 7, pp. 3622–3636, July 2013,
- [15] R. K. Hindustani, D. Dixit, and S. Sharma, "On the performance of multiple-IRS aided wireless networks over Nakagami-m fading channels," *International Journal of Communication Systems*, Aug. 2024. doi: 10.1002/dac.5945.
- [16] X. Li, X. Lian, X. Yue, Z. Lu, C. Huang, and T. Hou, "Performance Analysis of Double Reconfigurable Intelligent Surfaces Assisted NOMA Networks," *IEEE Transactions on Vehicular Technology*, vol. 73, no. 12, Dec. 2024.
- [17] Z. Abdullah, S. Kisseleff, K. Ntontin, W. A. Martins, S. Chatzinotas, and B. Ottersten, "Double-RIS Communication with DF Relaying for Coverage Extension: Is One Relay Enough?" in *Proc. IEEE International Conference on Communications (ICC)*, Seoul, South Korea, 2022, pp. 1–6, doi: 10.1109/ICC45855.2022.9839181.
- [18] J. Chen, K. Cao, H. Ding, L. Lv, Y. Ye, H. Chi, T. Wang, and L. Yang, "Double-RIS Enabled Physical Layer Security for Wireless-Powered Communication Systems Over Rayleigh Fading Channels," *IEEE Transactions on Communications*, vol. 73, no. 1, pp. xxx–xxx, Jan. 2025, doi: 10.1109/TCOMM.2025.3548690.
- [19] A. L. T. Le, H. T. Nguyen, T. V. Pham, and V. N. Q. Bao, "Performance Evaluation of Cooperative NOMA-IRS Network Using Particle Swarm Optimization," in *Proc. 2021 8th NAFOSTED Conference on Information and Computer Science (NICS)*, Hanoi, Vietnam, 2021, pp. 1–6, doi: 10.1109/NICS54270.2021.9701464.

APPENDIX:A

This Appendix derives the outage probability of the main communication link. The expression of the outage probability (OP) for D_1 is given as

$$\begin{aligned}\gamma_{D_1} &= \min\left(\gamma_{SR}^{(x_1)}, \gamma_{RD_1}^{(x_1)}\right) \\ \Rightarrow \gamma_{D_1} &= \min\left(\frac{P_S \alpha_1 g_{SR}}{P_S \alpha_2 g_{SR} + N_0}, \frac{P_R \alpha_1 g_{RD_1}}{I_{D_1} + N_0}\right).\end{aligned}$$

Now, the outage probability of D_1 is expressed as

$$\begin{aligned}P_{out}^{D_1} &= P\left(\min\left(\gamma_{SR}^{(x_1)}, \gamma_{RD_1}^{(x_1)}\right) < \gamma_{th}\right) \\ \Rightarrow P_{out}^{D_1} &= 1 - \underbrace{P\left(\gamma_{SR}^{(x_1)} \geq \gamma_{th}\right)}_{A_1} \cdot \underbrace{P\left(\gamma_{RD_1}^{(x_1)} \geq \gamma_{th}\right)}_{A_2}.\end{aligned}$$

Using probability statistics, A_1 and A_2 are derived as follows.

The SNR for the first Hop is expressed as:

$$\gamma_{SR}^{(x_1)} = \frac{P_S \alpha_1 g_{SR}}{P_S \alpha_2 g_{SR} + N_0} = \frac{\alpha_1}{\alpha_2 + \frac{N_0}{P_S g_{SR}}} \Rightarrow \text{Quasi-linear Function}$$

$$\gamma_{SR}^{(x_1)} < \gamma_{th} \Rightarrow g_{SR} < \frac{\gamma_{th} N_0 \lambda_{SR}}{(\alpha_1 - \alpha_2 \gamma_{th}) P_S}$$

$$\therefore P_{D_1}^{out} = P\left(\gamma_{SR}^{(x_1)} < \gamma_{th}\right) = P\left(g_{SR} < \underbrace{\frac{\gamma_{th} N_0 \lambda_{SR}}{(\alpha_1 - \alpha_2 \gamma_{th}) P_S}}_{\tau}\right)$$

$$\Rightarrow P_{out}^{D_1} = \frac{\gamma(N, \tau)}{\Gamma(N)} = \Gamma_{inc}(N, \tau)$$

Therefore,

$$A_1 = P(\gamma_{SR}^{(x_1)} \geq \gamma_{th}) = 1 - \Gamma_{inc}(N, \tau),$$

where, $\tau = \frac{\gamma_{th} N_0 \lambda_{SR}}{(\alpha_1 - \alpha_2 \gamma_{th}) P_S}$ and $\Gamma_{inc}(N, \tau)$ is the lower incomplete Gamma function.

The SNR for the second hop is expressed as:

$$\gamma_{RD_1}^{(x_1)} = \frac{P_R \alpha_1 g_{RD}}{I_{CD_1} + N_0} = \frac{\alpha_1 \xi P_S \beta \theta \eta g_{SR} g_{RD}}{(1 - \theta)(I_{CD_1} + N_0)} = \frac{K g_{SR} g_{RD_1}}{\sigma^2},$$

Now, define $g_{SR} g_{RD} > \frac{(1 - \theta)(I_{CD_1} + N_0) \gamma_{th}}{\alpha_1 \xi P_S \beta (1 - \theta) \eta} = K'$

An outage occurs if $g_{SR} g_{RD_1} < K'$. This is a product of two independent Gamma r.v.s. Thus, we use a Log-Normal approximation

let: $Z = X \cdot Y \sim \text{LogNormal}(2\mu_Z, 2\sigma_Z^2)$,

where, $\mu_Z = \log\left(\frac{N^2}{\sqrt{N^2 + N}}\right)$, $\sigma_Z^2 = \ln\left(1 + \frac{1}{N}\right)$.

Therefore,

$$P(Z < K') \approx \Phi\left(\frac{\ln(K') - 2\mu_Z}{\sqrt{2}\sigma_Z}\right)$$

$$\Rightarrow A_2 = P(\gamma_{RD_1}^{(x_1)} \geq \gamma_{th}) = 1 - \Phi\left(\frac{\ln(K') - 2\mu_Z}{\sqrt{2}\sigma_Z}\right) = Q\left(\frac{\ln(K') - 2\mu_Z}{\sqrt{2}\sigma_Z}\right),$$

Thus, the outage probability of D_1 is expressed as:

$$P_{out}^{D_1} = 1 - A_1 A_2 = 1 - \left[1 - \Gamma_{inc}\left(N, \frac{\gamma_{th} N_0}{(\alpha_1 - \alpha_2 \gamma_{th}) P_S \lambda_{SR}}\right)\right] \cdot \left[1 - \Phi\left(\frac{\ln(K') - 2\mu_Z}{\sqrt{2}\sigma_Z}\right)\right].$$

Similarly,

$$P_{out}^{D_2} = 1 - B_1 B_2,$$

where $B_1 = P(\gamma_{SR}^{(x_2)} \geq \gamma_{th}^D)$, $B_2 = P(\gamma_{RD_2}^{(x_2)} \geq \gamma_{th}^D)$.

Therefore,

$$P_{out}^{D_2} = 1 - \left[1 - \Gamma_{inc}\left(N, \frac{\gamma_{th}^D N_0}{\alpha_2 P_S \lambda_{SR}}\right)\right] \cdot \left[1 - \Phi\left(\frac{\ln(M') - 2\mu_Z}{\sqrt{2}\sigma_Z}\right)\right].$$

APPENDIX B

In this Appendix, we derive the analytical expression for the outage probability of the backscatter communication link. The SNR of the $C-R$ link is expressed as:

$$\gamma_{CR} = \frac{P_S(1-\beta)\xi(1-\theta)\alpha_1 g_{SR}g_{RC}g_{CR}}{N_0}.$$

Let

$$X = g_{SR} \sim \Gamma(N, \lambda_{SR}), \quad Y = g_{RC} \sim \exp(\lambda_{RC}), \quad Z = g_{CR} \sim \exp(\lambda_{CR}).$$

The outage probability is:

$$P_{\text{out}}^{CR} = P(\gamma_{CR} < \gamma_{th}^C) = P\left(XYZ < \frac{\gamma_{th}^C}{C}\right),$$

where, $C = \frac{P_S(1-\beta)\xi(1-\theta)\alpha_1}{N_0}$
Now consider $W = X.Y.Z$

$$\therefore f_W(w) = P(XYZ < w)$$

Since $W \sim \text{LogNormal}(\mu_W, \sigma_W^2)$

We have,

$$\mu_X = N, \quad \sigma_X^2 = N,$$

and

$$\mu_Y = 1, \quad \sigma_Y^2 = 1,$$

$$\mu_Z = 1, \quad \sigma_Z^2 = 1,$$

Therefore,

$$\mu_W = N \cdot 1 \cdot 1 = N, \quad \sigma_W^2 = 3N^2 + 4N$$

where,

$$\mu_W = \log\left(\frac{N^2}{\sqrt{4N^2 + 4N}}\right), \quad \sigma_W^2 = \log\left(4 + \frac{4}{N}\right).$$

$$\therefore P_{\text{out}}^{CR} \approx \Phi\left(\frac{\ln(K) - \mu_W}{\sigma_W}\right),$$

where

$$K = \frac{\gamma_{th}^C}{C} = \frac{\gamma_{th}^C}{P_S(1-\beta)\xi(1-\theta)}.$$

—

The SNR of the $R-C$ link is expressed as:

$$\gamma_{RC} = \frac{P_S(1-\beta)\xi g_{SR}g_{RC}}{N_0}.$$

Let $X = g_{SR} \sim \Gamma(N, \lambda_{SR}), \quad Y = g_{RC} \sim \exp(\lambda_{RC})$

$$\therefore \gamma_{RC} = C' \cdot X \cdot Y,$$

$$\text{where, } C' = \frac{P_S(1-\beta)\xi}{N_0}.$$

Thus, $P_{\text{out}}^{RC} = P(\gamma_{RC} < \gamma_{th}^C) = P\left(XY < \frac{\gamma_{th}^C}{C'}\right)$

Let $Z = XY$

We approximate:

$$Z \sim \text{LogNormal}(\mu_Z, \sigma_Z^2),$$

where

$$\mu_Z = \ln\left(\frac{N^2}{\sqrt{N^2 + 2N}}\right), \quad \sigma_Z^2 = \ln\left(1 + \frac{2}{N}\right).$$

Therefore,

$$P_{\text{out}}^{RC} \approx \Phi\left(\frac{\ln(K') - \mu_Z}{\sigma_Z}\right),$$

where, $K' = \frac{\gamma_{th}^C N_0}{\xi(1-\beta)P_S}$.

and $\Phi(\cdot)$ is the standard Gaussian cumulative distribution function (CDF).